

Particle Simulation Study of SOL Heat Transport to the Divertor Plate

Aaron FROESE¹⁾, Tomonori TAKIZUKA²⁾ and Masatoshi YAGI³⁾

¹⁾*IGSES, Kyushu University, Kasuga 816-8580, Japan*

²⁾*Japan Atomic Energy Agency, Naka 311-0193, Japan*

³⁾*RIAM, Kyushu University, Kasuga 816-8580, Japan*

(Received: 18 November 2009 / Accepted: 25 February 2010)

Parallel heat flux in a steady-state SOL is determined via fully kinetic simulations using the 1d3v particle-in-cell code PARASOL. In order to better evaluate the heat load on the divertor plates, the ion and electron velocity distributions functions (VDF), heat flux, and heat flux limiters α_i and α_e are calculated. The effects of collisionality, recycling rate, ion-electron mass ratio, and source model are examined. Results for the VDF are explained qualitatively and the average values of both flux limiters are found to be approximately 0.1, but with a large spread from $1.4 \times 10^{-3} \sim 2$ with a complex dependence on the simulation parameters.

Keywords: tokamak scrape-off layer, parallel heat transport, heat flux limiter, velocity distribution function, particle-in-cell

1. Introduction

In a tokamak, hot plasma is lost from the core by anomalous transport and ELMs and carried by parallel transport along the open field lines in the scrape-off layer (SOL) to the divertor plates. The SOL and plasma-surface interaction are highly complex features that need to be modeled numerically in order to simulate realistic fusion devices. Heat flux through the SOL must be regulated so as to limit heat loads on the divertor plates high enough to cause physical damage, necessitating lengthy and expensive maintenance. The most common approach is to model a 2d3v plasma with computationally fast fluid codes, but this requires that many kinetic factors be implemented manually, such as boundary conditions at the wall, heat conductivity, and plasma viscosity. Valid quantities must be acquired from fully kinetic simulations.

To accurately calculate energy-dependent sputtering rates, both the heat flux and velocity distribution function (VDF) at the sheath edge must be known. The parallel heat flux can be divided into the ion and electron conductive and convective heat fluxes,

$$q_{conv,\sigma} = n_\sigma m_\sigma \langle V_{\parallel,\sigma} v^2 \rangle / 2, \quad (1)$$

$$q_{cond,\sigma} = n_\sigma m_\sigma \langle (v_{\parallel} - V_{\parallel,\sigma}) v^2 \rangle / 2, \quad (2)$$

where v is the particle velocity, $V = \langle v \rangle$ is the fluid velocity, and brackets $\langle a \rangle \equiv \int a f_\sigma(x, \mathbf{v}) d\mathbf{v}$ indicate an average of the variable a over the phase-space distribution function f_σ of species $\sigma \in e, i$. Unlike the electron heat flux that is divided between convective and conductive, the ion heat flux is expected to be mainly convective [1]. The conductive heat flux is approximated by the Spitzer-Härm expression [2] in a

collisional plasma.

$$q_{SH,\sigma} = -\kappa_\sigma^{SH} \nabla_{\parallel} T_\sigma \quad (3)$$

$$\kappa_i^{SH} = 3.9 n_i v_{ti} \lambda_{ii} \quad \kappa_e^{SH} = 3.2 n_e v_{te} \lambda_{ee}$$

where κ_σ^{SH} is the heat conductivity, n_σ is the density, $v_{t\sigma} = (T_\sigma/m_\sigma)^{1/2}$ is the thermal speed, $\lambda_{\sigma\sigma} = v_{t\sigma} \tau_{\sigma\sigma}$ is the thermal mean free path (MFP), and $\tau_{\sigma\sigma} \propto v_{t\sigma}^3$ is the same-species collision time. This expression is valid when the actual heat flux is less than the order of the Maxwellian one-way free-streaming heat flux

$$q_{FS,\sigma} = n_\sigma T_\sigma (T_{\parallel,\sigma}/m_\sigma)^{1/2}, \quad (4)$$

where $T_{\parallel,\sigma} = n_\sigma^{-1} \int dv \cdot v_{\parallel}^2 f_\sigma(x, v)$ is the temperature parallel to the magnetic field. The collision-dependent heat flux is approximated via the harmonic mean [3],

$$q_{eff,\sigma} = \left(\frac{1}{q_{SH,\sigma}} + \frac{1}{\alpha_\sigma q_{FS,\sigma}} \right)^{-1}, \quad (5)$$

where the flux-limiting coefficient $\alpha_\sigma \equiv \lim_{\lambda_{mfp} \rightarrow \infty} q_\sigma / q_{FS}$ is defined as the ratio between the actual heat flux and the one-way free-streaming heat flux in the collisionless limit. The heat flux limiters are usually assumed to be $\alpha_\sigma \approx 0.1$, although previous kinetic simulations have given values in the range $\alpha_i = 0.1 \sim 2$ and $\alpha_e = 0.03 \sim 3$ [1].

We have studied the heat transport in SOL plasmas with the PARASOL code and shown that in a collisionless plasma where the ion-electron mass ratio is $m_i/m_e = 400$, the electron heat flux limiter is $\alpha_e = 0.75$ in a plasma at equilibrium [4]. Further exploration showed that for a more realistic mass ratio of $m_i/m_e = 1800$, α_e varies smoothly from a very small value when the electron radiation energy-loss rate is low to approximately unity when it is high [5]. In addition, examination of the effect of collisionality has

author's e-mail: aaron@riam.kyushu-u.ac.jp

shown that when there is no electron radiation, the heat flux does not follow a harmonic average transition from the collisional to the collisionless state, but peaks at moderate collisionalities when the mean free path is of the order of the system length and then decreases to the collisionless limit. The reason for the decrease was found to be the development of a large high-energy tail in the electron energy distribution as the plasma becomes more collisionless [6]. The tail effect is overpowered when electron radiation creates an asymmetry between the incoming and outgoing electron distributions, thereby raising the heat flux in the collisionless limit and eliminating the peak. Adding a Langevin heat bath model to the source region was also found to suppress the tail asymmetry, preventing formation of the peak.

These previous studies have concentrated on the response of the electron heat flux to collisionality, electron radiation rate, and the type of source model. In contrast, this work investigates the behaviour of the ion heat flux in response to different mass ratios and recycling rates, as well as collisionality and source model effects.

2. Simulation model

The PARASOL code simulates a 1d3v self-consistent electrostatic particle-in-cell model with a binary collision model [4, 7]. A slab geometry is used with motion on the separatrix parallel to the magnetic field. Position in the toroidal direction is given by coordinate x (Fig. 1). Ions are fully traced (1d3v), electrons follow their guiding centers (1d2v), and for this study neutrals are ignored. The ratio of the poloidal magnetic field to the total field strength is set to $\Theta = B_x/B = 0.2$. The ion gyro-radius is set to $\rho_i/L = 5 \times 10^{-3}$, the number of spatial cells to 800, and the number of ions to $N_0 = 10^6$. The time step length in the runs presented is the inverse of the plasma frequency, $\Delta t = \omega_{pe}^{-1}$. Each run requires approximately $K = 1 \times 10^5$ time steps to reach equilibrium, which takes approximately 10 hours on 12 modern CPUs. Equilibrium data is acquired by averaging over time from $K = 1.8 \times 10^5$ to 2.0×10^5 .

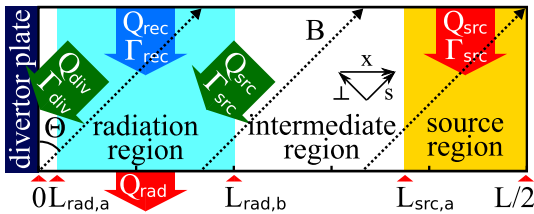


Fig. 1 Half the simulation domain showing source/sink regions, magnetic field, and flux values.

The spatial domain is symmetric across the midpoint, with divertor plates located at $x = 0$ and $x = L$.

There is no difference between inboard and outboard divertor plates to avoid masking the heat flux physics we wish to observe. The half-domain shown in Fig. 1 is divided into three major regions: source, intermediate, and radiation/recycling. The source region lies in the center, where hot particles are generated and a Langevin heat bath may also be employed. In the Langevin model, each particle j lying within the source region experiences heating given by the Langevin equation,

$$\frac{\Delta \mathbf{v}_j}{\Delta t} = -\nu \mathbf{v}_j + A, \quad \langle A^2 \rangle = 2 \frac{T_{L0}}{m_j} \frac{\nu}{\Delta t}, \quad (6)$$

where ν is the Langevin relaxation constant, A is a random variable of uniform distribution with range set by the given temperature T_{L0} , and m_j is the particle mass. The heating parameters are $\nu \Delta t = 10^{-3}$ and $T_{Li0} = T_{Le0} = T_{e0}$. The Langevin model ensures that the velocity distribution tends towards Maxwellian even in a collisionless plasma with poor mixing [6]. The radiation/recycling regions lie near the divertor plates, where an electron energy sink and an ambipolar cold particle source model radiative cooling and recycling, respectively. Explanation of the radiation model is given in [7]. In this case, the radiation energy-loss fraction is set to $f_{rad} = Q_{rad}/Q_{src} = 0.6$. Between the source and radiation regions lie the intermediate regions, where sampling occurs. As reported by others [8], the values of α_σ vary by orders of magnitude along the field line, so the poloidal average over the intermediate region is taken.

Ions lost to the divertor plates are replaced at the hot particle and cold recycling sources. Particle generation is ambipolar, so electron and ion source fluxes are equal, $\Gamma_{src,e} = \Gamma_{src,i}$, $\Gamma_{rec,e} = \Gamma_{rec,i}$. Since the source particle flux is equal to the ion flux to the divertor, a sheath potential forms and a positive bias develops in the plasma bulk. The ratio of recycling to hot source particle generation is an input parameter $R = \Gamma_{rec,\sigma}/(\Gamma_{src,\sigma} + \Gamma_{rec,\sigma})$. Hot particles are generated uniformly within the source region $L_{src,a} = 0.4L < x < L/2$, with an isotropic thermal distribution of temperature $T_{e0} = T_{i0} = 1$. Cold particles are generated uniformly within the recycling region $L_{rec,a} = 0.01L < x < 0.21L = L_{rec,b}$, with an isotropic thermal distribution of temperature $T_{rec,e}/T_{e0} = 5 \times 10^{-3}$, $T_{rec,i}/T_{e0} = 1 \times 10^{-3}$.

3. Results and discussion

The effects of four different properties are explored: the mean free path is given a value of $\lambda_{mfp,i} \sim L$ for a moderately collisionless SOL and $\lambda_{mfp,i} \sim 10^3 L$ for a very collisionless SOL, the recycling rate is given a value of 0% or 99%, the Langevin heat bath can be absent or present, and the ion-electron mass ratio is varied between $m_i/m_p = 1$ to mimic a hydro-

genic plasma and 4 to mimic an impure plasma, where $m_p/m_e = 1800$ is the proton mass. The electron and ion VDF are averaged over the range $x = [0 : 0.09]$ which includes the sheath edge. We confirm that the inclusion of the entire sheath region in the averaging does not change the VDF significantly, because the ranges $x = [0 : 0.09]$ and $x = [0.09 : 0.18]$ give similar results. The effects of the former three properties are shown in Fig. 2 for the case with $m_i/m_p = 1$. At first glance, we see that the electrons are generally composed of two Maxwellian populations [5]: the bulk that are trapped by the sheath potential and a high-energy tail of electrons that travel directly from the hot source to the divertor plate. Despite not being trapped, the ions also have a bulk population and high-energy tail, which we have difficulty explaining, especially in the case of a collisionless plasma.

By comparing the moderately collisional VDF in Figs. 2 (a,c,e,g) to the corresponding collisionless plasma in Figs. 2 (b,d,f,h), we see that the temperature of the bulk populations of both electrons and ions is greatly reduced as mixing is reduced, since the tendency to return to a thermal distribution is eliminated. Less heat is transferred from the hot source particles to the bulk as they travel to the divertor. This leaves more and more electrons trapped in the radiation regions, reducing the electron heat flux to the divertor plate and hence the flux at the source (as confirmed in Fig. 3), decreasing the plasma potential. At equilibrium, electron and ion loss is ambipolar, so the ion flow rate to the divertor also decreases, despite reduced backscatter by the ions.

Fig. 2 (a,b,e,f) and (c,d,g,h) show a comparison of the ion and electron VDF for the case of 0% recycling versus 99% recycling. The addition of recycling reduces the ion temperature and flow rate at the sheath edge, while concurrently increasing the electron temperature. The reduced ion temperature and flow rate naturally occurs because of the cold recycled ions entering the plasma in the radiation/recycling region. The effect is amplified as the collisionality increases and the recycled ions cool more of those directly from the source. Just as electron radiation creates a low-energy population of electrons and reduces the electron heat flux, recycling creates a distinct population and significantly reduces the ion heat flux to the divertor. However, if the origin of the bulk distribution is cool, recycled ions, it is unusual that the bulk temperature is many times larger than that of the recycled ions, even without mixing. This must be investigated further. Electron temperature increases because the recycled electron temperature is higher relative to the recycled ion temperature ($T_{rec,e} = 5T_{rec,i}$) and the electron radiation rate is very high (60%). Once electrons from the source reach the sheath region, they are already cooler than the recycled electron temperature.

If the radiation model was deactivated, both ions and electrons would experience an decreased temperature and flow rate due to recycling.

To see the effect of the heat source model, we compare heating using only the hot particle source in Fig. 2 (a-d) with runs that also include Langevin heating in Fig. 2 (e-h). The Langevin heat bath increases overall heating and forces the particles towards a thermal distribution. Since it affects all particles within the source region, mixing behavior occurs even in a collisionless plasma. In all cases, the fluid velocity and heat flux towards the divertor plate increase, as seen in Figs. 3 and 4. The density of particles in the high-energy tail also increases relative the total density. Due to the bath, the temperature in the source region stabilizes at a high value, which increases the total heat flux and reduces its susceptibility to other factors.

Heat fluxes corresponding to each VDF in Fig. 2 with and without Langevin heating are shown in Figs. 3 and 4, respectively. These figures also show dependence of the heat fluxes on the ion-electron mass ratio. The mass ratio is found to introduce a small, smoothly varying effect on the heat flux that typically varies over only a factor of 2, equivalent to the change in $(m_i/m_e)^{1/2}$. The only exception is the ion conductive heat flux, which increases by up to 1 order of magnitude as the ion mass grows from $m_i/m_p = 1$ to 4. A greater ion mass should raise the sheath potential according to the relation $e\phi_e/T_e \simeq 1/2 \ln m_i/m_e$, which traps a larger fraction of the electrons and raises the bulk electron temperature. This further increases the sheath potential, which helps to accelerate the ions to the divertor. However, we can see that ion conduction is not always dominated by convection.

Other effects on the heat flux follow directly from the VDF. As the collisionality is reduced, when thermalizing behaviour is not alternatively provided by Langevin heating, the ion conductive heat flux increases and electron heat flux is reduced. This corresponds to the higher ion flow velocity and reduced electron temperature. Recycling reduces the ion temperature and increases the electron temperature, so the heat fluxes likewise decrease and increase, respectively. Langevin heating increases the particle temperature across the board, and so the heat fluxes also increase prodigiously.

The value of α_i and α_e for each set of conditions is shown in Table 1. The left half shows the result of using only the hot particle source. In this case, the strongest effect is caused by collisionality. There is an increase of 1 order of magnitude in α_e and 2 orders in α_i when going from a moderately collisional plasma to a low collisional plasma. Without recycling, both limiters have a weak dependence on the mass ratio close to $\alpha_\sigma \propto (m_e/m_i)^{1/2}$. However, with 99% recycling,

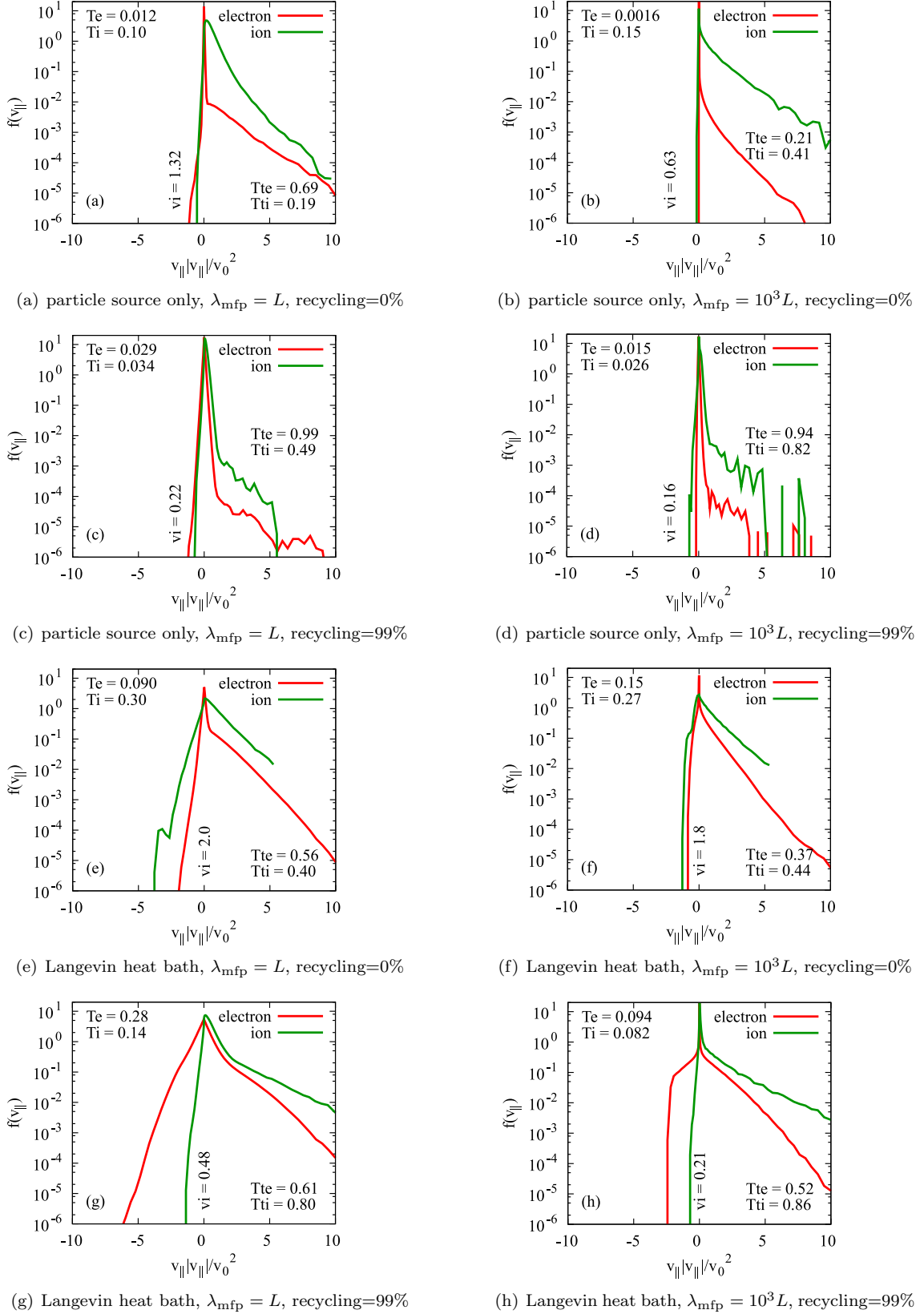


Fig. 2 Ion and electron distribution functions of random energy (fluid velocity removed) averaged over the region $x/L=[0:0.09]$ for different collisionalities, recycling rates, and either a hot particle or Langevin heat sources. Average temperatures (T_i , T_e), tail temperatures ($T_{t,i}$, $T_{t,e}$), and ion fluid velocities (v_i) are labelled.

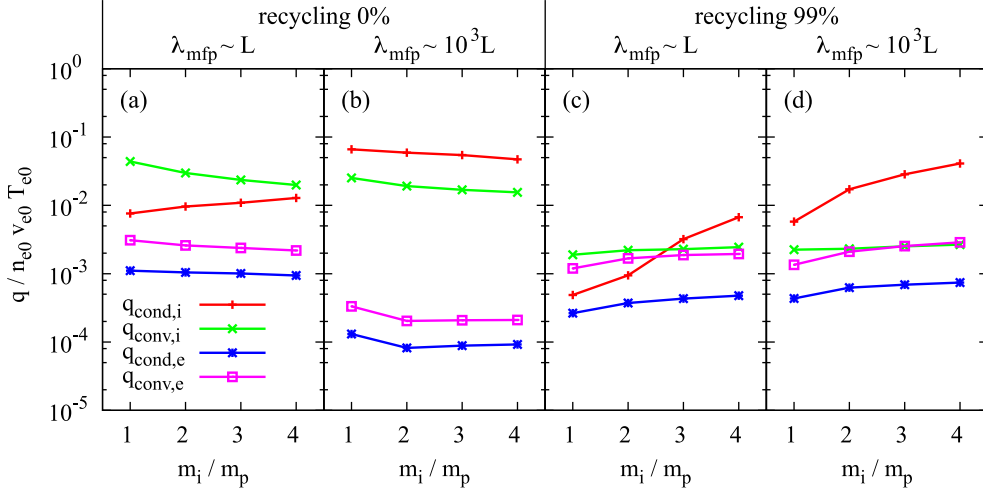


Fig. 3 Hot particle source only case: mass dependence of ion conduction (+), ion convection (x), electron conduction (*), and electron convection (\square) heat fluxes measured at the sheath edge.

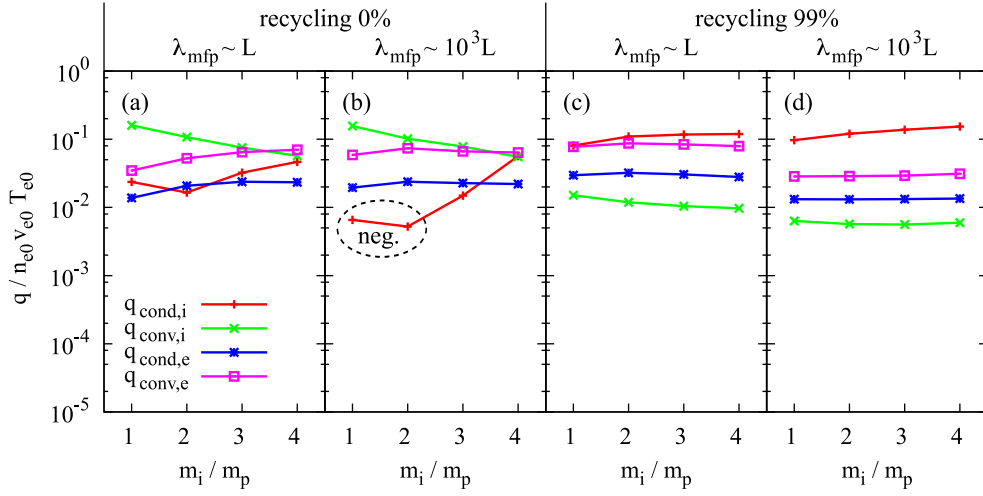


Fig. 4 Langevin heating case: mass dependence of ion conduction (+), ion convection (x), electron conduction (*), and electron convection (\square) heat fluxes measured at the sheath edge. Negative values (circled) are plotted by magnitude.

parameters			hot particle source only		Langevin heating	
λ_{mfp}/L	R	m_i/m_p	α_e	α_i	α_e	α_i
1	0.00	1	1.0×10^{-1}	4.5×10^{-3}	3.9×10^{-1}	3.8×10^{-2}
1	0.00	2	7.0×10^{-2}	2.2×10^{-3}	3.8×10^{-1}	4.4×10^{-2}
1	0.00	3	5.5×10^{-2}	1.8×10^{-3}	3.5×10^{-1}	1.6×10^{-2}
1	0.00	4	4.6×10^{-2}	1.4×10^{-3}	2.7×10^{-1}	1.4×10^{-2}
1	0.99	1	1.4×10^{-2}	3.2×10^{-3}	2.8×10^{-1}	7.0×10^{-2}
1	0.99	2	1.0×10^{-2}	3.9×10^{-3}	1.7×10^{-1}	3.5×10^{-2}
1	0.99	3	8.7×10^{-3}	4.0×10^{-3}	1.3×10^{-1}	2.4×10^{-2}
1	0.99	4	7.3×10^{-3}	4.2×10^{-3}	1.1×10^{-1}	1.8×10^{-2}
10^3	0.00	1	7.4×10^{-1}	2.4×10^{-1}	7.2×10^{-1}	4.8×10^{-2}
10^3	0.00	2	5.1×10^{-1}	1.8×10^{-1}	5.4×10^{-1}	4.3×10^{-2}
10^3	0.00	3	4.0×10^{-1}	1.4×10^{-1}	3.7×10^{-1}	5.0×10^{-2}
10^3	0.00	4	3.5×10^{-1}	1.1×10^{-1}	3.1×10^{-1}	6.5×10^{-2}
10^3	0.99	1	7.8×10^{-2}	2.2×10^{-1}	1.1	1.8
10^3	0.99	2	3.9×10^{-2}	4.2×10^{-1}	6.7×10^{-1}	1.6
10^3	0.99	3	2.4×10^{-2}	5.3×10^{-1}	4.7×10^{-1}	1.4
10^3	0.99	4	3.1×10^{-2}	5.5×10^{-1}	3.6×10^{-1}	1.3

Table 1 Heat flux limiters α_σ measured at $x/L = [0.27 : 0.36]$ for different collisionality, recycling rate, ion-electron mass ratio, and source model.

this trend reverses itself for α_i , switching instead to a small increase with mass ratio. The inclusion of recycling decreases α_e by about 1 order of magnitude.

The right half of Table 1 shows the result of Langevin heating. The overall effect is to increase and stabilize the heat flux limiters. Without the Langevin heating, α_i lies in the range $[1.4 \times 10^{-3} : 0.55]$, but with heating, the range becomes $[1.4 \times 10^{-2} : 1.8]$. Likewise for the electron heat flux limiter, α_e goes from the range $[7.3 \times 10^{-3} : 0.35]$ to $[0.11 : 1.1]$. In both cases, the maximum and minimum increase by more than an order of magnitude and their ratio becomes less than half as much as for the hot particle source only case. Because of the additional heating, collisionality becomes less important, with the collisionless SOL giving a slightly higher value for both limiters by a small factor ~ 1 . Going from small to large mass ratio ($m_i/m_p = 1$ to 4) causes α_e to decrease, and causes α_i to decrease in two cases: when there is neither recycling nor Langevin heating and when there is both recycling and Langevin heating. This is because the presence of either recycling or Langevin heating creates a strong temperature gradient, making the ion conductive heat flux very sensitive to the mass ratio.

Since the flux limiters α_σ are defined as the ratio of the actual heat flux to the one-way free-streaming heat flux according to Eq. 5, they are most affected by changes to the shape of the actual velocity distribution. Looking at the VDF in Fig. 2, we see the distributions typically become more symmetric by decreasing the recycling rate, increasing collisionality, or using Langevin heating. The electron distribution reacts somewhat more strongly to the changes than the ion distribution. We can deduce that α_σ is increased by conditions that cause an irregularly-shaped VDF: *increasing* the recycling rate, *decreasing* collisionality, or *deactivating* Langevin heating. Table 1 confirms that this assumption is correct for the collisionality condition and for the heating method condition, except for the collisionless case without recycling where both α_e and α_i become much larger when Langevin heating is activated. In fact, it is seen that adjusting the plasma collisionality is the most efficient way to increase α_i and especially α_e . The recycling condition does not lend itself to such clear analysis. (Note that one cannot technically make a direct comparison between Fig. 2 and the Table 1, because the sampling regions are next to the divertor ($x/L = [0 : 0.09]$) and inside the intermediate region ($x/L = [0.27 : 0.36]$), respectively. However, only the distribution of electrons proceeding away from the divertor is significantly different, and usually only at low velocity.)

4. Summary

To better evaluate the heat load on the divertor plates, the ion and electron VDF, as well as the ion and electron heat flux and heat flux limiters α_i and α_e were examined. Both ion and electron VDF were found to have high-energy tails separate from low-energy bulk populations, but for different reasons. The tails derive from the hot particle source, while the electron bulk is due to trapping by the sheath. The ion bulk is strengthened by recycling, but also occurs in the absence of recycling. Collisionality and Langevin heating are found to force the plasma towards a thermal distribution, but the former reduces flow rate and heat flux, while the latter increases them. Recycling reduces the ion temperature, flow rate, and heat flux. Finally, the effects of the ion-electron mass ratio are small, except when a strong temperature gradient can be induced with recycling or Langevin heating.

The average values of the flux limiters α_σ are found to be approximately 0.1, as currently employed in fluid codes. However, they show a wide deviation from 1.4×10^{-3} to 2 for only the tested simulation parameters, so the actual variation is likely even greater. Therefore, using a constant value is not recommended. At the very least, some linear correction should be employed to account for changes to the ion-electron mass ratio, recycling rate, collisionality, and heating model. As already pointed out [8], α_σ even varies by orders of magnitude along the field line, a detail which we corroborate. Ultimately, limiting the heat flux may provide no substantial benefits. Therefore, future work should be directed to developing a more accurate model for incorporation in fluid codes. In addition, fluid codes require a number of other kinetic factors, including the heat transmission coefficients, ion viscosity, sheath potential, and polytropic constant. Further inquiry will be directed towards the effect of the plasma parameters on these factors.

- [1] W. Fundamenski. *Plasma Phys. Control. Fusion*, 47(11):R163–R208, 2005.
- [2] S. I. Braginskii. *Transport processes in a plasma*, volume 1. Consultant Bureau, New York, 1965.
- [3] Peter C. Stangeby. *The Plasma Boundary of Magnetic Fusion Devices*. Taylor & Francis, New York, 2000.
- [4] T. Takizuka, M. Hosokawa, K. Shimizu. *Trans. Fusion Technol.*, 39:111–118, 2001.
- [5] A. Froese, T. Takizuka, M. Yagi. Electron parallel heat transport in the scrape-off layer using a particle-in-cell code. *to be published in Plasma Fusion Res.*
- [6] A. Froese, T. Takizuka, M. Yagi. Effect of source and sink on heat transport in the SOL. *to be published in Contrib. Plasma Phys.*
- [7] T. Takizuka, K. Tani, M. Azumi, K. Shimizu. *J. Nucl. Mater.*, 128:104–110, 1984.
- [8] D. Tskhakaya et al. *Contrib. Plasma Phys.*, 48(1-3):89–93, 2008.